Since January 2020 Elsevier has created a COVID-19 resource centre with free information in English and Mandarin on the novel coronavirus COVID-19. The COVID-19 resource centre is hosted on Elsevier Connect, the company's public news and information website.

Sensors & Actuators: B. Chemical 369 (2022) 132379

Contents lists available at ScienceDirect

Sensors and Actuators: B. Chemical

journal homepage: www.elsevier.com/locate/snb

Mask assistance to colorimetric sniffers for detection of Covid-19 disease using exhaled breath metabolites

Mohammad Mahdi Bordbar [a], Hosein Samadinia [a], Ali Hajian [b], Azarmidokht Sheini [c], Elham Safaei [d], Jasem Aboonajmi [d], Fabiana Arduini [e], Hashem Sharghi [d], Pegah Hashemi [f], Hosein Khoshsafar [a], Mostafa Ghanei [a], Hasan Bagheri [a,*]

[a] Chemical Injuries Research Center, Systems Biology and Poisonings Institute, Baqiyatallah University of Medical Sciences, Tehran, Iran
[b] Institute of Sensor and Actuator Systems, TU Wien, Gusshausstrasse 27-29, 1040 Vienna, Austria
[c] Department of Mechanical Engineering, Shohadaye Hoveizeh Campus of Technology, Shahid Chamran University of Ahvaz, Dashte Azadegan, Khuzestan, Iran
[d] Department of Chemistry, College of Sciences, Shiraz University, Shiraz, Iran
[e] Department of Chemical Science and Technologies, University of Rome Tor Vergata, Via della Ricerca Scientifica, 00133 Rome, Italy
[f] Research and Development Department, Farin Behbood Tashkhis LTD, Tehran, Iran

ARTICLE INFO

Keywords:
Breath analysis
Covid-19 detection
Colorimetric sniffers
Non-invasive methods
Coronavirus
Metabolomics

ABSTRACT

According to World Health Organization reports, large numbers of people around the globe have been infected or died for Covid-19 due to the severe acute respiratory syndrome coronavirus 2 (SARS-CoV-2). Researchers are still trying to find a rapid and accurate diagnostic method for revealing infected people by low viral load with the overriding goal of effective diagnostic management. Monitoring the body metabolic changes is known as an effective and inexpensive approach for the evaluation of the infected people. Here, an optical sniffer is introduced to detect exhaled breath metabolites of patients with Covid-19 (60 samples), healthy humans (55 samples), and cured people (15 samples), providing a unique color pattern for differentiation between the studied samples. The sniffer device is installed on a thin face mask, and directly exposed to the exhaled breath stream. The interactions occurring between the volatile compounds and sensing components such as porphyrazines, modified organic dyes, porphyrins, inorganic complexes, and gold nanoparticles allowing for the change of the color, thus being tracked as the sensor responses. The assay accuracy for the differentiation between patient, healthy and cured samples is calculated to be in the range of 80%—84%. The changes in the color of the sensor have a linear correlation with the disease severity and viral load evaluated by rRT-PCR method. Interestingly, comorbidities such as kidney, lung, and diabetes diseases as well as being a smoker may be diagnosed by the proposed method. As a powerful detection device, the breath sniffer can replace the conventional rapid test kits for medical applications.

1. Introduction

Based on the World Economic Forum report, the development of breath sensors for rapid detection of diseases is one of the ten emerging technologies that will be highly regarded by researchers and commercial companies in the next two to five years [1]. Exhaled breath is composed of many volatile metabolites, which are classified into amines, ketones, acids, aldehydes, and carbohydrates [2]. The variation in the metabolism concentrations indicates a physiological disorder in the human body, eventually leading to the lung, kidney, and gastrointestinal diseases, airway inflammation, and metabolic disorders (e.g., diabetes, obesity, nonalcoholic fatty liver disease, and hyperlipidemia) [3].

So far, the breath metabolites have been estimated using standard laboratory methods such as gas chromatography (GC) [4], spectroscopic methods including mass spectrometry (MS) [5], proton transfer reaction mass spectrometry (PTR-MS) [6], laser spectroscopy [7], ion mobility spectrometry and/or a combined approach of GC and MS [8]. These methods provide the sufficient information about the type and the amount of metabolites in infected, healthy, and even cured patients. Different metabolic profiles for each sample arise from the appearance, removal, and a concentration change of a certain metabolite [9].

By the advent of SARS-CoV-2 in 2019, and the widespread epidemic

* Corresponding author.
E-mail address: h.bagheri@bmsu.ac.ir (H. Bagheri).

https://doi.org/10.1016/j.snb.2022.132379
Received 29 April 2022; Received in revised form 12 July 2022; Accepted 13 July 2022
Available online 14 July 2022

Covid-19 as a contagious respiratory disease [10], several studies have been performed to evaluate and compare the exhaled breath compositions of Covid-19 patients, healthy people, and individuals infected with other acute respiratory diseases. In this regard, the values of some chemical compounds such as 2, 4-octadiene 1-chloroheptane, nonanal, ethanal, octanal, acetone, butanone, and methanol in the metabolic profiles of the patients infected by Covid-19 have been reported to be different from those by other respiratory disorders [11,12]. The discrimination of healthy samples from the Covid-19 patients were obtained by evaluating the changes in the concentration of some volatile species, consisting of 1-propanol, 3, 6-methylundecane, camphene, beta-cubebene, and iodobenzene [13,14].

Determination of the trace amounts of volatiles, and creation of a unique and reliable response for each exhaled breath sample are the most important features of conventional methods. Nevertheless, collecting virus-infected samples, and transferring them to an isolated clinical laboratory are cumbersome using the instrumental methods. Moreover, they suffer from the involvement of large, expensive and complex instruments with a skilled personnel to set them up. The consumption of an excessive volume of materials or reagents, together with the lack of rapid responses are considered as other limitations of these methods.

A suitable alternative is the use of the multiplexed nanomaterial-based sensor developed by Shan et al. In fact, this is an electronic nose (E-nose) system, consisting of eight gold nanoparticles (AuNPs; modified with thiol compounds) embedded in an electrical circuit [15]. This system can detect and differentiate between the breath metabolites of patients, healthy people and patients with non-Covid respiratory diseases, providing accuracy in the range of 90%—94% [15]. Another similar study by Nurputra et al. has described the performance of a commercial E-nose (GeNose C19), comprising an array of metal oxide semiconductors for discriminating between the breath volatile compounds of healthy and patient volunteers with the assistance of various pattern recognition methods [16]. The suggested assay represented the classification results with accuracy of 88%—95% [16]. Having a simple design, the portability and the possibility of on-site sampling are the advantages of E-nose-based systems. Also, the sensor response, derived from an alteration in the electrical resistance of the sensing elements, can be shown digitally to the users [17]. However, the E-nose systems have some disadvantages such as their complex, delicate and costly electrical circuits that may need to be repaired. Furthermore, weak van der Waals interactions occur between the metabolites and the array components of E-nose sensors. The relative humidity of the reaction medium can have a negative effect on the sensor responses as well [18, 19].

The possibility of using optical electronic noses (opto-E-noses) has been reported for several applications, including the evaluation of the quality of food and water, monitoring of drugs and explosive values, determination of ions and anions, and detection of fungi, bacteria, and cancerous tissues [20–27]. These E-noses employ colorimetric indicators for binding to the volatile compounds through Lewis donor-acceptor, Bronsted acid-base, charge transfer, and H-bonding interactions [20].

The opto-E-noses have been utilized in the diagnosis of diseases such as lung cancer [28] and sinusitis (via exhaled breath metabolites) [29], leukemia (via whole blood metabolites) [24], and urinary tract infection (via urinary metabolites) [22]. These arrays are made of porphyrins, organic dyes, and salts or functionalized gold and silver NPs immobilized on a polymer substrate such as polyvinylidene difluoride (PVDF) [20]. The sampling for colorimetric breath analysis can be performed by collecting the volatile metabolites in a bag, followed by injecting them into the sensor array chamber using an external pump or an inert gas stream [28]. Therefore, it is possible that the device is not usable for on-site analysis, and that enough metabolites do not exist in the collected sample or the sample is not correctly passed on the sensor surface.

In a hierarchical process, we sought to develop the rapid diagnostic tools for the detection of Covid-19 disease by monitoring the metabolites of exhaled breath and biological samples. Our previous study reported an electronic tongue based on colorimetric method for recognizing of chemical markers in the saliva samples of this patients and healthy population. The device discriminated patients infected by Covid-19 from healthy controls with a accuracy of 84.0% [30]. The present study proposes an opto-E-nose which is directly exposed to exhaled breath metabolites using a thin face mask without the need of the external force for transferring the sample to the surface of the sensor. The device is compose of the low-cost general filter paper, whose configuration comprises a diverse set of sensing elements such as porphyrazines, porphyrins, AuNPs, metal ion complexes, and modified organic dyes. This design allows for the measurement of a variety of volatiles, while also increasing the sensor selectivity for recognizing a specific chemical compound, and determining the samples at low concentrations with high sensitivity. Overall, the opto-E-nose is expected to provide a favorable response for differentiating the Covid-19 patients from healthy controls and cured samples, and to have the high ability to simultaneously find the metabolites of other comorbidities. Also, the assay is examined for making a semi-quantitative relationship between the disease severity and the color changes of sensing components.

2. Experimental section

2.1. Instruments and software

Designing and printing the pattern of the proposed sensor was performed by AutoCAD 2016 software and HP LaserJet printer 1200, respectively. A canon scanner (CanoScan LiDE 220) was used to capture the sensor photos. The resulting images were processed by Image J (1.51 n, National Institutes of Health, USA). Statistical data processing was carried out by MATLAB R2015 and SPSS (Version 22; Chicago, IL, USA) software. The sensing components were spotted on the surface of paper by a micropipette (BRAND Transferpette® S, Germany). To control the pH of media, a Metrohm 632 pH-meter (Model 780 pH lab) was used.

2.2. Materials and solutions

The organic dyes such as bromophenol red (R1), acridine orange (R2), indigo carmine (R3), toluidine blue (R4), malachite green (R5), phenol red (R6), pararosaniline hydrochloride (R7), thymol blue (R8), methyl red (R9), bromophenol blue (R10), bromopyrogallol red (R11), methyl blue (R12), pyrocatechol violet (Py), gallic acid (GA) and the chemicals like sodium citrate, bovine serum albumin (BSA), polyvinyl pyrrolidone (PVP), 2, 4-dinitrophenylhydrazine, phenylboronic acid (PBA), p-toluenesulfonic acid monohydrate (TsOH), tetrabutylammonium hydroxide (TBAOH), vanadyl sulfate pentahydrate ($VOSO_4.5\ H_2O$) were obtained from Sigma Aldrich. The other compounds consist of bromocresol purple (R13), gold (III) chloride trihydrate ($HAuCl_4.3\ H_2O$), sodium borohydride ($NaBH_4$), sodium hydroxide (NaOH), ethanol (EtOH), sulfuric acid (H_2SO_4), nickel(II) nitrate hexahydrate ($Ni(NO_3)_2.6\ H_2O$), copper(II) nitrate trihydrate ($Cu(NO_3)_2.3\ H_2O$), iron(II) chloride tetrahydrate ($FeCl_2.4\ H_2O$), iron(III) nitrate nonahydrate ($Fe(NO_3)_3.9\ H_2O$) and boric acid (H_3BO_3) were provided from Merck chemical company. The pattern of sensor was drawn on the Whatman® Grade NO.2 filter paper. The water soluble tetramethyl quaternized tetracationic porphyrazines (tetramethyl tetra-3,4-pyridinoporphyrazinato cobalt(II) $[Co(3,4\text{-tmtppa})]^{4+}$, tetramethyl tetra-2,3-pyridinoporphyrazinato copper(II) $[Cu(2,3\text{-tmtppa})]^{4+}$, tetramethyl tetra-3,4-pyridinoporphyrazinato zinc(II) $[Zn(3,4\text{-tmtppa})]^{4+}$, tetramethyl tetra-3,4-pyridinoporphyrazinato iron(II) (Fe(2,3-tmppa))) as well as porphyrines ([*meso*-tetraphenylporphyrin] iron(III) chloride (Fe(III)TPPCl), *meso*-tetrakis(4-chlorophenyl) porphyrin-manganese(III) acetate (Mn(III)T(4-Cl)PP(OAC)), *eso*-tetrakis(4-hydroxyphenyl) porphyrin-manganese(III) acetate (Mn(III)T(4-OH)PP(OAC)), [*meso*-

tetraphenylporphyrin]-copper(II) (Cu(II)TPP) and [*meso*-tetraphenylporphyrin]-tin(II) (Sn(II)TPP)) were synthesized using procedures have been reported previously [31–36]. The sterile thin cloth and three-layer medical masks were prepared from a mask production center in Tehran, Iran.

2.3. Study population

This study was performed in Baqiyatallah Hospital, Tehran, Iran between 2020 and 2021. Same as our previous study [30], the participants were selected from 21 to 80 years . 60 Covid-19 patients whose disease was confirmed by a pulmonologist, and the results of their chest x-ray and rRT-PCR tests were positive, were admitted to this study [30]. These patients did not take any medicine before the admission to the hospital. 55 volunteers of the other medical clinics were chosen as controls who had not been infected by Covid-19 before this study. 15 cured samples were invited to participate in the re-analysis after two months. All experiments were clearly explained to the volunteers. They were asked to sign an informed consent for participating in this study. The medical document of each individual was collected. The demographic information is summarized in Table S1 [30].

2.4. Sensor fabrication

To prepare the paper sensor, the desired pattern was first designed with AutoCAD software, and then printed on a filter paper substrate. The pattern shown in Fig. 1a consists of a square hydrophobic zone (black areas) and 32 circular hydrophilic zones (white areas). The hydrophobic areas were created by the penetration of the printer ink into the texture of the paper, while also blocking the paper holes [37]. This was achieved by placing the printed paper in an oven at 200 °C for 45 min [37]. To fabricate the sensor array, 0.2 μL of each color indicator (Fig. 1b) was dropped on a hydrophilic substrate (Fig. 1c). The location and contents of each sensing component are shown in Fig. 1b. The developed sensor was pasted onto the center of a plastic strip with size of 2.5 × 5.5 cm (see Scheme 1a-b). The sides of the strip were covered with double-sided adhesive (Scheme 1c). Note that the strip used had good flexibility and mechanical stability.

2.5. Colorimetric detection process

A sterile package containing a sensor array, a thin cloth, and a three-layer medical mask was given to each participant. First, the thin cloth mask was placed on the face (Scheme 1d). The double-sided adhesive was then removed (Scheme 1e). The sensor was stuck to the face mask (Scheme 1 f), and covered with the three-layer medical mask to prevent the physical interference and environmental pollutions (Scheme 1 g). The participant was asked to normally perform the inhalation and exhalation cycles for a certain period of time without any external force (Scheme 1 h). During this time, the participant could continue his daily activities (except sleeping and eating). The exhaled breath metabolites directly interacted with the sensing components, resulting in discoloration of the indicators. These changes were observed by the naked eye (Scheme 1i). The color responses were recorded by a scanner, and analyzed by the image analysis software (Scheme 1j). For each sensing component, the outputs were three numerical values obtained from the difference of the mean values of R, G and B color elements. The difference value was calculated by subtracting the RGB values of the primary sensor from those of the reacted sensor. In total, a vector of 96 data points (32 sensing components × 3 color elements) was obtained for each participant.

2.6. Statistical evaluation of data

To verify the sensor ability to discriminate between the two studied classes of patient-healthy, patient-cured and healthy-cured categories, three matrices with sizes of (115 × 96), (75 × 96) and (70 × 96) were prepared, respectively. Statistical analysis of pattern recognition was performed by principle component analysis-linear discriminate analysis (PCA-LDA) in MATLAB environment. Statistical parameters such as the sensitivity, specificity, accuracy and error rate were calculated for all the three categories. To obtain the total sensor response for each participant, the norm of the data vector known as the Euclidean norm, was calculated as follows:

$$Euclidean \quad Norm = \sqrt{\sum_{i=1}^{n} (x_i)^2}$$

where x_i is the ith numerical value of the data vector. Equation (1) was also used to estimate the total response of a sensing component, involving a data vector with three values related to the RGB color elements.

Two independent sample t-tests were used to compare between the average values of the total sensor responses obtained from the patient and healthy groups. The correlation between the total response of the sensor (or the total response of a sensing component) and other parameters such as age, O_2 saturation, disease severity and viral load value was investigated by the Pearson correlation coefficient. SPSS software was employed to run this statistical analysis.

3. Results and discussion

A sniffer was developed based on a colorimetric sensor array for the detection of exhaled breath volatile metabolites, according to the experimental section. The ability of the sensor to discriminate the patients with Covid-19 from the healthy people was evaluated. The following subsections describe the results of the assay in detail.

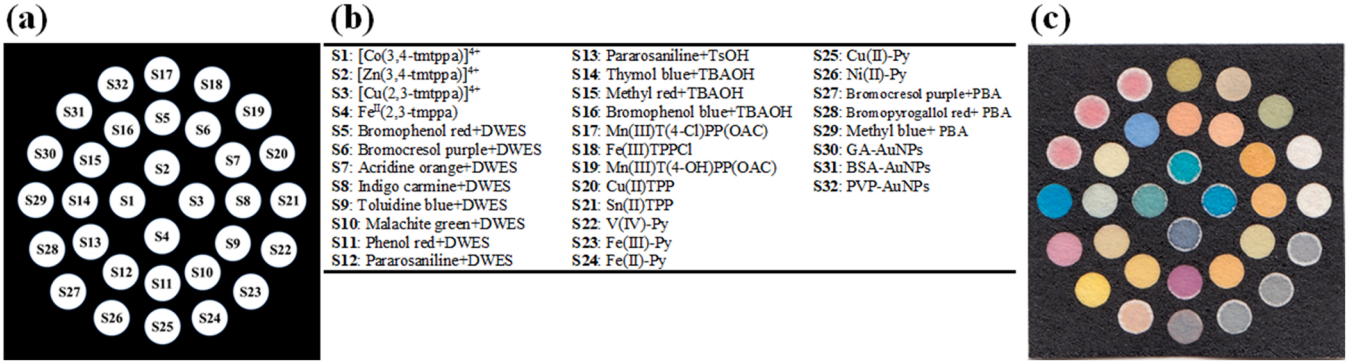

Fig. 1. (a) The schematic pattern of sensor designed by AutoCAD, (b) the names of sensing elements and their locations and (c) the image of fabricated sensor array.

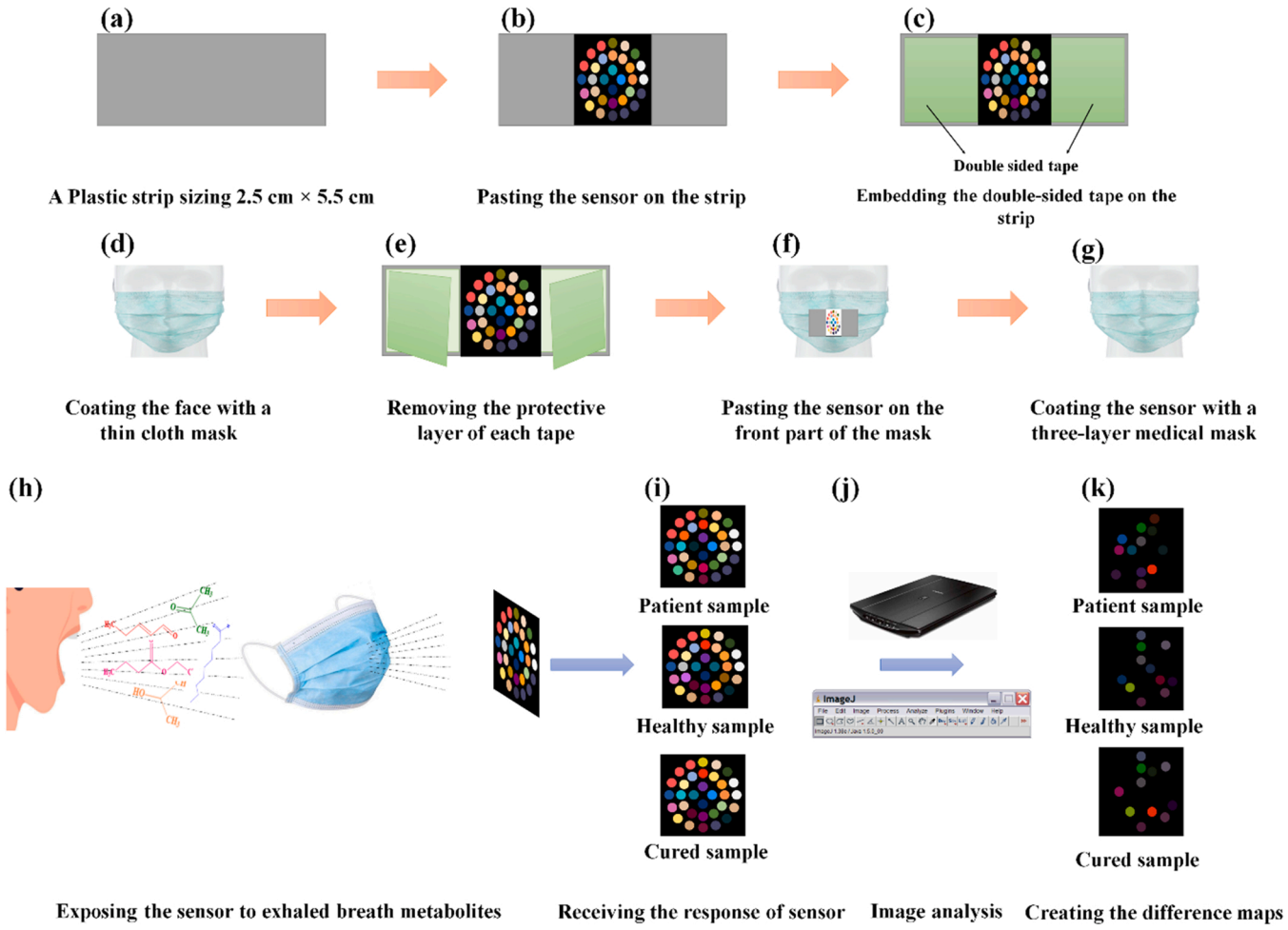

Scheme 1. The schematic diagram for fabrication and application of colorimetric sniffer device: (a) providing a plastic strip with the size of 2.5 cm × 5.5 cm, (b) pasting the sensor on the strip, (c) embedding the double-sided tape on the strip, (d) coating the face with a thin cloth mask, (e) removing the protective layer of each tape, (f) pasting the sensor on the front part of the mask, (g) coating the sensor with a three-layer medical mask, (h) exposing the sensor to exhaled breath metabolites, (i) receiving the response of sensor, (j) capturing the image by a scanner and processing the image by image analysis software and (k) creating the colorimetric difference maps.

3.1. Optimization

The array structure consists of the colorimetric components such as porphyrazines, organic dyes, porphyrins, metal ion complexes, and NPs. The organic dyes can also be combined with additives such as DWES, TBAOH, TsOH and PBA. The amount of each compound and the volume ratio of organic dye: additives in the resultant mixture can affect the sensor response. As well, the time required for the interaction between the metabolites and sensor components must be calculated. These evaluations were performed by optimization experiments in order to find maximum values of the total response of the sensor.

To find the optimal value of each indicator, four different experimental models were designed while Model 1 and Model 4 containing the lowest and highest amounts of colorimetric components, respectively (Fig. S1a). As can be seen in Fig. S1b, the strongest interaction between the metabolites and the sensor components, together with the best sensor response is achieved by using Model 3 for preparing the indicator solutions. The lower values of the indicator are not sufficient to complete the reaction, and the higher values prevent the monitoring of the changes arising from the interactions [38].

In the next step, the organic dyes were mixed with the additives in different volume ratios of (1:1), (2:1), (3:1), (4:1), and (5:1), as seen in Fig. S1c. The results presented in Fig. S1d show that the color changes of the sensing components become more intense with increasing the contribution of the organic dye in the mixture (thus decreasing the additive contribution). In this respect, the highest response is obtained using the volume ratio of (4:1). It is worth noting that the desired reaction does not occur at the lower amount of the additives, and the active sites of indicators are blocked using high amounts of these materials.

Volatile metabolites must be given time to distribute throughout the sensor surface, and interact with its sensing components. The analysis will be stopped once the color changes of all the indicators are fixed, being indicative of the completion of the reaction. Fig. S1e shows that 75 min is required to carry out a desirable experiment.

3.2. Sensor outputs

The discrimination between the patients with Covid-19 disease, the healthy individuals, and other people with non-Covid lung diseases arises from the changes of volatile compounds in the exhaled breath samples [14]. These chemicals are classified in the alkanes, alkenes, aldehydes, ketones, acids, alcohols, and arenes categories [14]. The array components interact with all the volatile metabolites through Lewis acid-base, Bronsted acid-base, electrostatic, H-bonding, charge transfer, π-π, dipole-dipole, and hydrophobic interactions, although color changes may be observed with different intensities depending on the type and amount of the chemical species [20]. Metalloporphyrins

and metalloporphyrazines participant in the Lewis acids- bases adduct formation, being attached to analytes by transferring the non-bonding electron pairs [39]. The response of these sensing elements is influenced by the chemical properties of the central metal, the strict hindrance of the macrocyclic aromatic structure,the polarity, chemical hardness, and affinity of the analytes [40]. Unlike porphyrins, the porphyrazines contain meso nitrogen atoms, and have a high potential for participation in nucleophilic and H-bonding reactions [41]. In other word, the presence of four electron acceptor pyridine rings in the structure of porphyrazines, dramatically increase the Lewis acidity of their metal centers and conclusively, increasing their tendency for adduct formation by analyte. Organic dyes are proton donors or acceptors whose color highly depends on the pH of media [42]. To increase reactivity, the organic dyes are mixed with specific additives. Among these substances, DWES tends to do a nucleophilic attack to the carbonyl species [43], whereas PBA binds to diols [44]. The products of both reactions change the concentration of H_3O^+. Alternatively, TsOH provides the conditions for the interaction between aniline-containing dyes and aldehydes through the Schiff test reaction [45]. Moreover, TBAOH is used to induce facile proton transfer reactions [46]. Metal ion complexes can be employed as sensing elements for metabolite detection. In this case, the analyte replaces the ligand in the complex structure (i.e., the indicator displacement assay) or is simultaneously attached to the ligand and the metal ion, resulting in the formation of a ternary compound [47]. The stability constant of the metal-ligand complex, and the affinity of the metal ion to the analyte, are the two main factors for this interaction [48]. AuNPs can detect volatile species with a detection limit of 10 ppb [49]. The NP-based arrays provide the fingerprint patterns for chemical materials with different functional groups. The modification of NPs with various capping agents such as GA, BSA, and PVP allows them to interact with a wide range of analytes through electrostatic, H-bonding, and covalent interactions, leading to the color changes of the sensor from red to purple due to the NP aggregation [49].

The proposed sensor array contains 32 chemical compounds related to porphyrazines, porphyrins, the organic dyes mixed with DWES, TsOH, TBAOH and PBA, metal ion complexes, and AuNPs. The sensor was exposed to the volunteer exhaled breath metabolites, and the corresponding colorimetric responses were collected after 75 min. The results obtained by the colorimetric and the image analyses of patient, healthy and cured participants are shown in Fig. 2a. All observations are collected in Fig. S2-S4. Also, due to the interaction of the analyte with the sensing component, the partial color changes are clearly represented by the color difference maps (Fig. 2b).

Among all the array components, while S2 ($[Zn(3,4\text{-tmtppa})]^{+4}$), S5 (Bromophenol red + DWES) and S25 (Cu(II)-Py) respond to the volatile metabolites of all the studied samples, no color changes are observed for S4 (FeII (2,3-tmppa)), S7 (Acridine orange + DWES), S16 (Bromophenol blue + TBAOH), S20 (Cu (II) TPP), S21 (Sn (II) TPP), S24 (Fe (II) - Py), S26 (Ni (II)-Py), S28 (Bromopyrogallol red + PBA), S29 (Methyl blue + PBA), and all the NPs (S30–S32). It is indicated that the color of $[Co(3,4\text{-tmtppa})]^{+4}$ (S1) and $[Cu(2,3\text{-tmtppa})]^{+4}$ (S3) is turned on in the colorimetric profiles of the patient and healthy samples, respectively. DWES-organic dyes, including bromocresol purple (S6), indigo carmine (S8), malachite green (S10), and phenol red (S11) have a high tendency towards volatile compounds in the patient's exhaled breath. The markers such as toluidine blue (S9) and pararosaniline (S12) interact with the metabolites of healthy individuals. The dyes combined with TsOH (S13) tend to interact with volatile markers in healthy individuals, whereas TBAOH-integrated indicators (S14 and S15) become discolored in the presence of infected breath samples. Among porphyrins, only Fe (III) TPPCl (S18) responds to the patient metabolites. Both metalloporphyrins with the central metal Mn (S17–S19), and the metal ion complexes of V (IV) and Fe(III) (S22 and S23) are illuminated in the color profile of the healthy individual. Although S27 (Bromocresol purple + PBA) is sensitive to the chemical species of the sample with Covid-19, other PBA-organic dyes are not influenced by the breath compositions of these studied groups.

In order to evaluate the treatment process, patients (15 samples) were asked to participate in this study once again after complete recovery. The test conditions were the same as before. As shown in Fig. 2, the sensor response to the volatile metabolites of the cured samples is different from that obtained by healthy and infected volunteers. The sensing components S1, S8, S11, S15, S18, and S27 are turned off in the color map of the cured samples. In this case, the metabolites responsible for changing the color of these sensors are possibly removed from the exhaled breath profile. However, one can observe the discoloration of S6, S10, and S14, indicating that the body's metabolic behavior is still affected by the viral infection. Interestingly, some dedicated sensing elements for the healthy samples such as S12, S17, S19, S22 and S23 appear in the color profile of the cured participants, evidencing the progress in the treatment process as well as the accession of the normal situation.

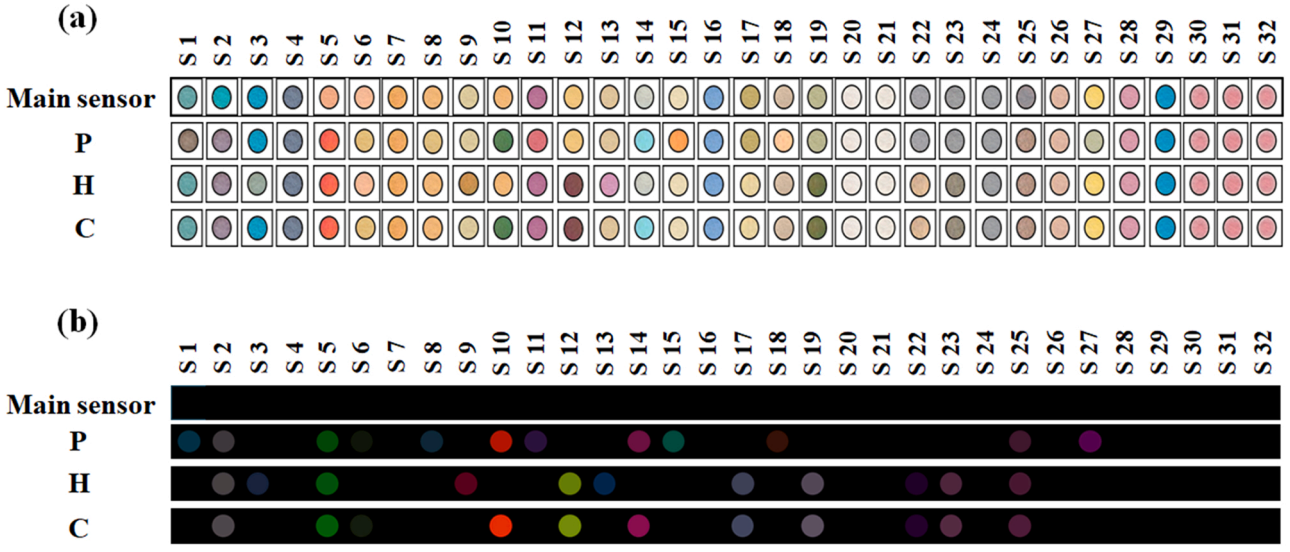

Fig. 2. (a) The colorimetric response and (b) the colorimetric difference maps of fabricated sensor for patient infected by Covid-19 (P), Healthy control (H) and Cured sample (C). The data was capture after 75 min and at the optimum conditions reported in Fig. S1.

3.3. Discrimination of population

The sensor efficiency in the creation of a difference pattern between the studied samples was evaluated using unsupervised pattern recognition methods such as PCA. For statistical analysis, three different sets, including patient-healthy, patient-cured, and healthy-cured were prepared by forming a data matrix with sizes of (115 × 96), (75 × 96), and (70 × 96), respectively. The score plots obtained by PCA analysis are summarized in Fig. 3, and the classification statistical parameters are collected in Table 1.

Fig. 3a shows the discrimination pattern obtained for the patient-healthy matrix data. The total variance extracted from the first two principal components (PCs) is 93.73%. Accordingly, 47 patients and 46 healthy people with a 95% confidence level are located in the correct sets, whereas 9 patients and 7 healthy samples are misdiagnosed . In total, 6 people (4 patients and 2 healthy samples) are not classified in any group. The parameters obtained from PCA show that the colorimetric method can discriminate the patients from healthy people with a

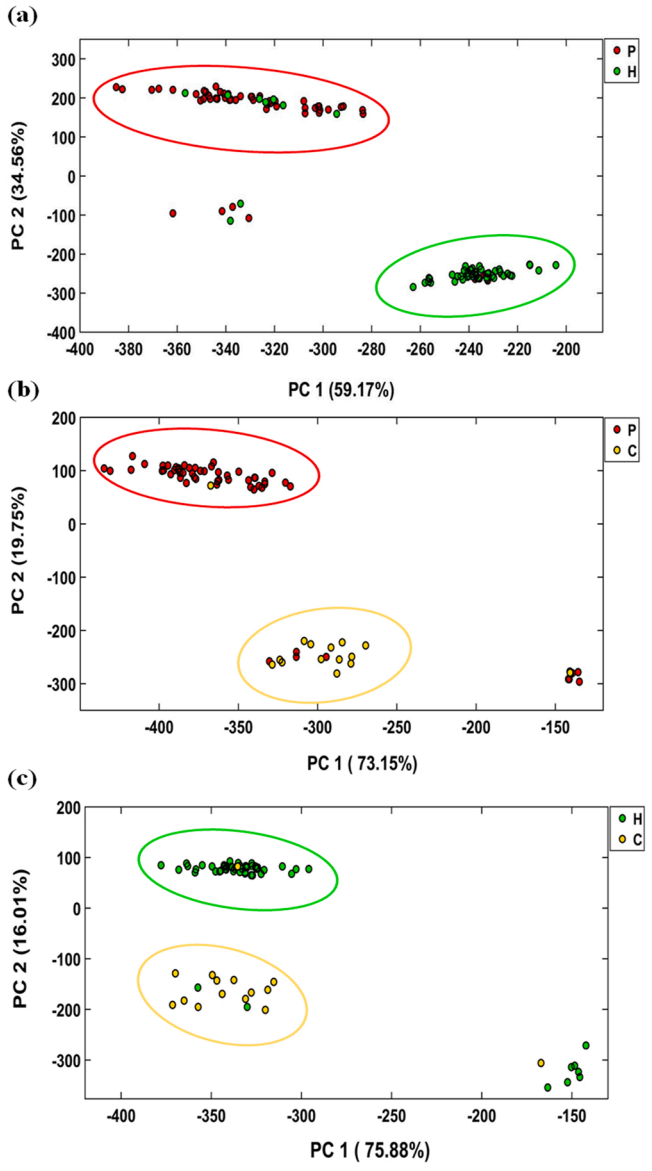

Fig. 3. The score plots obtained by PCA analysis for three different matrices including the data of patients and healthy samples (a), patients and cured samples (b) and healthy and cured samples (c). The data was capture after 75 min and at the optimum conditions reported in Fig. S1.

Table 1
Classification results obtained by PCA-LDA analysis.

Parameters	Patient vs Healthy	Patient vs Cured	Healthy vs Cured
Sensitivity (%)	78.3	78.3	83.6
Specificity (%)	83.6	86.6	86.6
Accuracy (%)	80.8	80.0	84.3
Error rate (%)	19.2	20.0	15.7

sensitivity of 78.3%, and specificity of 83.6%. The accuracy of the method was calculated to be 80.8%.

The ability of the sensor to differentiate between patient and cured participants is shown in Fig. 3b. The first two PCs comprise 92.9% of the total explained variances. The results reveal that 47 patients and 13 cured samples are correctly diagnosed with a confidence level of 95%. However, 4 infected and 1 cured volunteers fall into the opposite categories. The sensor responses for 9 patients and 1 cured sample are similar to those for the healthy ones. Table 1 illustrates that the proposed method is able to differentiate between members of this set, having the sensitivity and specificity of 78.3% and 86.6%, respectively. In this case, the accuracy was found to be 80%.

For the last set (healthy-cured), the PCA diagrams depicted in Fig. 3c indicate that 91.9% of the total variance is distributed over the first two PCs. This method can classify 46 healthy and 13 cured people with a 95% confidence level. Among the remaining participants, 3 samples are clustered incorrectly, and 8 samples are not placed in the two classes. As seen in Table 1, the sensitivity, specificity and accuracy of this discrimination are equal to 83.6%, 86.6% and 84.3%, respectively.

It should be noted that the adverse sensor responses can be due to the errors in the sampling process, improper transfer of chemical markers from the mask cavities into the sensor texture and low concentration of the markers in the exhaled breath profile due to the mildness of the disease.

3.4. Diagnosis of disease severity

The participants were divided into the following 5 groups based on their disease severity: very mild, mild, moderate, severe, and very severe. The disease severity was determined by a pulmonologist using the vital signs, symptoms, chest imaging, and rRT-PCR results. The total responses of the sensor array and each sensing component were quantified. As illustrated in Fig. 4a, the color of the sensing element (S8) considerably changes by severity of the disease. As depicted in Table S2, an acceptable and significant relationship between these variables is observed due to the high Pearson coefficient (0.946) and low P (<0.001) values.

On the other hand, the relationship between the response of sensory components and viral load value (extracted from the rRT-PCR analysis based on the number of N gene cycle threshold (CT)) was investigated. To this end, the results of PCR were categorized in four sets: low, moderate, high and very high. As is clear in Fig. 4b and Fig. 4c, the response of sensing components (S15 and S27) shows an increasing trend with increasing the viral load value. The Pearson coefficients of 0.922 and 0.931 are obtained for S15 and S27, respectively, according to Table S2. As a result, the PCR analysis information can be qualitatively estimated using the proposed colorimetric sniffer.

3.5. Comorbidities detection

Volunteers may be smokers or have other non-Covid diseases such as cardiovascular disease, chronic kidney disease, asthma, diabetes, chronic obstructive pulmonary disease, chronic liver disease, and hypertension. Metabolites of these diseases can also appear in the breath profile.

Considering the previous studies, volatile compounds such as

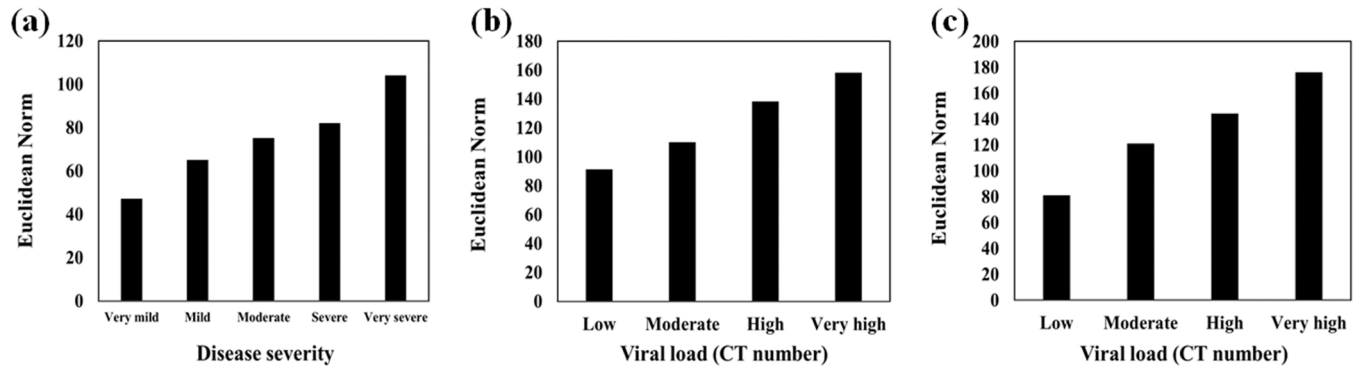

Fig. 4. (a) The correlation between the response of S8 and disease severity, (b) and (c) the relationship of S15 and S27 responses with the viral load obtained by rRT-PCR analysis, respectively. The data was capture after 75 min and at the optimum conditions reported in Fig. S1.

acetonitrile and furan derivatives (for smokers) [50], amines and ammonia (for people with chronic kidney disease) [51], acetone, ethanol and methyl nitrate (for diabetics) [52], and isoprene, 4, 7-dimethyl -undecane, 2,6-dimethyl-heptane, acetaldehyde, 2-butyl octanol and methyl isobutyrate (for people with lung disorders) [53] have been reported as effective metabolites for differentiating between the relevant disease and normal cases. For participants of this study, the corresponding comorbidities are listed in Table S1. The developed sensor was exposed to the exhaled breath of people with these diseases. Fig. S5 shows the colorimetric response and colorimetric maps of patients with Covid-19, being smokers or having kidney, diabetes, or lung disorders. As can be seen, the interaction between the exhaled breath of people with diabetes and the sensor components results in the discoloration of S28 (Bromopyrogallol red + PBA). The kidney disease metabolites tend to interact with S16 (Bromophenol blue + TBAOH) and S31 (BSA-AuNPs). Acridine orange + DWES (S7) responds to volatile compounds in smokers. Finally, the color of Sn (II) TPP (S21) and Fe (II)-Py(S 24) appears in the difference maps of participants with asthma and COPD. The diagnosis ability of the sensor for detection of these diseases is determined to be 85.0% for smokers, 86.6% for kidney disease, 75.0% for diabetes and 75.0% for lung disorders.

Consider that the metabolites of other diseases do not interact with sensing elements that respond to COVID-19 related markers. Also, the specified sensing components turned on in the presence of metabolites of a particular disease. Thus, the proposed sensor provide a unique response for a certain disease.

3.6. Statistical points

The Euclidean norm of the data vector provided by the image analysis was calculated as the total response for each studied sample. The mean of responses for each of patient and healthy groups was equal to 387.88 (± 33.11) and 361.29 (± 22.34), respectively. For all patient and healthy data, the total average was 375.17 (± 31.33). The results of two independent t-tests confirmed that the mean value obtained by the patient samples was higher than that by healthy ones. Thus, the difference obtained (26.59) was statistically significant (P-value <0.001). It can also be concluded that the Euclidean norm of higher than the total average value (375.17) is indicative of the patient sample, whereas the response of the sensor for a healthy participant has a lower value than the total average.

Furthermore, the effect of age and O_2 saturation was investigated on the sensor response. The results of the correlation test between the total response and age of volunteers (Table S3) show that the value of Pearson correlation coefficient is calculated to be 0.024 for patients, and 0.061 for healthy individuals. The corresponding P-values are obtained to be 0.855 and 0.657, giving rise to the lack of a significant relationship between the two variables. From Table S3, no strong and significant correlation is observed between the total response and O_2 saturation of all the volunteers. The Pearson correlation coefficient and P-value are 0.117 and 0.395 for the patient group, and 0.178 and 0.192 for the healthy samples. These results explain that the colorimetric response depends on the metabolic changes of the exhaled breath, and is not affected by other variables.

4. Conclusions

For the first time, the diagnosis of a patient with Covid-19 has been performed based on the analysis of exhaled breath metabolites using a colorimetric sniffer. Compared to standard detection methods, the proposed assay was user-friendly because of its simplicity, and low-cost design and fabrication process, as well as being portable and capable of on-site detection. By this method, the volatiles were directly exposed to the sensor without the need of separate and tedious sampling process, providing more desirable sensitivity compared to the PCR method. Unlike the current diagnostic methods, the proposed assay showed high ability to discriminate the cured samples from healthy people, and to detect the comorbidities such as kidney disease, diabetes, and lung disorders, together with their disease severity. This sensor can be easily used in hospitals, medical laboratories, homes, shops, factories and public transportation to identify the disease vectors. The design of the colorimetric breath sensors with the same experimental procedure for detection of other diseases is underway in our research group.

CRediT authorship contribution statement

Mohammad Mahdi Bordbar: Project administration, Methodology, Investigation, Formal analysis, Writing – original draft. **Hosein Samadinia**: Conceptualization, Design, Validation, Resources. **Ali Hajian**: Methodology, Validation, Writing – review & editing. **Azarmidokht Sheini**: Methodology, Validation. **Elham Safaei**: Conceptualization, Methodology, Validation. **Jasem Aboonajmi**: Methodology, Validation. **Fabiana Arduini**: Conceptualization, Writing – review & editing. **Hashem Sharghi**: Conceptualization, Validation. **Pegah Hashemi**: Methodology, Validation. **Hosein Khoshsafar**: Methodology, Validation. **Mostafa Ghanei**: Conceptualization, Methodology, Validation, Resources. **Hasan Bagheri**: Supervision, Conceptualization, Methodology, Writing – review & editing.

Data availability

Data will be made available on request.

Acknowledgement

The authors gratefully acknowledge the support from Research Council of Baqiyatallah University of Medical Sciences, Tehran, Iran.. Also, The authors would like to thank the Clinical Research

Development Unit of Baqiyatallah Hospital, for all their support and guidance during carrying out this study.

Declaration of competing interest

The authors declare the following competing financial interest(s): Five authors (Mohammad Mahdi Bordbar (M.M.B.), Pegah Hashemi (P. H.), Hosein Khoshsafar (H. Kh.), Mostafa Ghanei (M. Gh) and Hasan Bagheri (H. B)) have filed a provisional patent application on the technology described in this manuscript entitled "A colorimeric sniffer for qualitative and quantitative detection of Covid-19 disease". The remaining authors declare that they have no competing interests.

Compliance with Ethical Standards

The research ethics committee of Baqiyatallah University of Medical Sciences has approved the project (Approval ID: IR.BMSU.REC.1399.508).

Appendix A. Supporting information

Supplementary data associated with this article can be found in the online version at doi:10.1016/j.snb.2022.132379.

References

[1] M. DiChristina, B. Meyerson, These are the top 10 emerging technologies of 2021, World Econ. Forum (2021) 1–2. ⟨https://www.weforum.org/agenda/2020/11/2020-top-10-emerging-technologies/⟩.

[2] V.R. Nidheesh, A.K. Mohapatra, V.K. Unnikrishnan, R.K. Sinha, R. Nayak, V. B. Kartha, S. Chidangil, Breath analysis for the screening and diagnosis of diseases, Appl. Spectrosc. Rev. 56 (2021) 702–732, https://doi.org/10.1080/05704928.2020.1848857.

[3] T. Chen, T. Liu, T. Li, H. Zhao, Q. Chen, Exhaled breath analysis in disease detection, Clin. Chim. Acta 515 (2021) 61–72, https://doi.org/10.1016/j.cca.2020.12.036.

[4] M. Zhou, R. Sharma, H. Zhu, Z. Li, J. Li, S. Wang, E. Bisco, J. Massey, A. Pennington, M. Sjoding, R.P. Dickson, P. Park, R. Hyzy, L. Napolitano, C. E. Gillies, K.R. Ward, X. Fan, Rapid breath analysis for acute respiratory distress syndrome diagnostics using a portable two-dimensional gas chromatography device, Anal. Bioanal. Chem. 411 (2019) 6435–6447, https://doi.org/10.1007/s00216-019-02024-5.

[5] L. Bregy, Y. Nussbaumer-Ochsner, P. Martinez-Lozano Sinues, D. García-Gómez, Y. Suter, T. Gaisl, N. Stebler, M.T. Gaugg, M. Kohler, R. Zenobi, Real-time mass spectrometric identification of metabolites characteristic of chronic obstructive pulmonary disease in exhaled breath, Clin. Mass Spectrom. 7 (2018) 29–35, https://doi.org/10.1016/j.clinms.2018.02.003.

[6] Y. Sun, Y. Chen, C. Sun, H. Liu, Y. Wang, X. Jiang, Analysis of volatile organic compounds from patients and cell lines for the validation of lung cancer biomarkers by proton-transfer-reaction mass spectrometry, Anal. Methods 11 (2019) 3188–3197, https://doi.org/10.1039/c9ay00759h.

[7] B. Henderson, A. Khodabakhsh, M. Metsälä, I. Ventrillard, F.M. Schmidt, D. Romanini, G.A.D. Ritchie, S. te Lintel Hekkert, R. Briot, T. Risby, N. Marczin, F. J.M. Harren, S.M. Cristescu, Laser spectroscopy for breath analysis: towards clinical implementation, Appl. Phys. B Lasers Opt. 124 (2018), https://doi.org/10.1007/s00340-018-7030-x.

[8] C. Steppert, I. Steppert, T. Bollinger, W. Sterlacci, Rapid non-invasive detection of Influenza-A-infection by multicapillary column coupled ion mobility spectrometry, J. Breath Res. (2020), https://doi.org/10.1101/2020.06.04.20099259.

[9] D.J. Beale, F.R. Pinu, K.A. Kouremenos, M.M. Poojary, V.K. Narayana, B. A. Boughton, K. Kanojia, S. Dayalan, O.A.H. Jones, D.A. Dias, Review of recent developments in GC–MS approaches to metabolomics-based research, Metabolomics 14 (2018), https://doi.org/10.1007/s11306-018-1449-2.

[10] WHO, Laboratory testing for 2019 novel coronavirus (2019-nCoV) in suspected human cases, WHO - Interim Guid. 2019 (2020) 1–7.

[11] S. Grassin-Delyle, C. Roquencourt, P. Moine, G. Saffroy, S. Carn, N. Heming, J. Fleuriet, H. Salvator, E. Naline, L.J. Couderc, P. Devillier, E.A. Thévenot, D. Annane, Metabolomics of exhaled breath in critically ill COVID-19 patients: a pilot study, EBioMedicine 63 (2021), https://doi.org/10.1016/j.ebiom.2020.103154.

[12] D. Ruszkiewicz, D. Sanders, R. O'Brien, F. Hempel, M.J. Reed, A.C. Riepe, J. K. Baillie, E. Brodrick, K. Darnley, R. Ellerkmann, O. Mueller, A. Skarysz, M. Truss, T. Wortelmann, S. Yordanov, P. Thomas, B. Schaaf, M. Eddleston, Diagnosis of COVID-19 by analysis of breath with gas chromatography-ion mobility spectrometry: a feasibility study, SSRN Electron. J. (2020), https://doi.org/10.2139/ssrn.3675407.

[13] W. Ibrahim, R.L. Cordell, M.J. Wilde, M. Richardson, L. Carr, A.S.D. Dasi, B. Hargadon, R.C. Free, P.S. Monks, C.E. Brightling, N.J. Greening, S. Siddiqui, Diagnosis of covid-19 by exhaled breath analysis using gas chromatography–mass spectrometry, ERJ Open Res. 7 (2021), https://doi.org/10.1183/23120541.00139-2021.

[14] H. Chen, X. Qi, J. Ma, C. Zhang, H. Feng, M. Yao, Breath-borne VOC biomarkers for COVID-19, MedRxiv (2020), https://doi.org/10.1101/2020.06.21.20136523.

[15] B. Shan, Y.Y. Broza, W. Li, Y. Wang, S. Wu, Z. Liu, J. Wang, S. Gui, L. Wang, Z. Zhang, W. Liu, S. Zhou, W. Jin, Q. Zhang, D. Hu, L. Lin, Q. Zhang, W. Li, J. Wang, H. Liu, Y. Pan, H. Haick, Multiplexed nanomaterial-based sensor array for detection of COVID-19 in exhaled breath, ACS Nano 14 (2020) 12125–12132, https://doi.org/10.1021/acsnano.0c05657.

[16] D. Nurputra, A. Kusumaatmadja, M. Hakim, S. Hidayat, T. Julian, B. Sumanto, Y. Mahendradhata, A. Saktiawati, H. Wasisto, K. Triyana, Fast and noninvasive electronic nose for sniffing out COVID-19 based on exhaled breath-print recognition, ResearchSquare (2021). ⟨http://www.epistemonikos.org/documents/f9d96eb0a964ef0fa3c19ec1fa0d2981b892caa7⟩.

[17] H.Y. Yang, W.C. Chen, R.C. Tsai, Accuracy of the electronic nose breath tests in clinical application: a systematic review and meta-analysis, Biosensors 11 (2021), https://doi.org/10.3390/bios11110469.

[18] W.J. Harper, The strengths and weaknesses of the electronic nose, Adv. Exp. Med. Biol. 488 (2001) 59–71, https://doi.org/10.1007/978-1-4615-1247-9_5.

[19] N.S. Ramgir, Electronic nose based on nanomaterials: issues, challenges, and prospects, ISRN Nanomater. 2013 (2013) 1–21, https://doi.org/10.1155/2013/941581.

[20] Z. Li, J.R. Askim, K.S. Suslick, The optoelectronic nose: colorimetric and fluorometric sensor arrays, Chem. Rev. 119 (2019) 231–292, https://doi.org/10.1021/acs.chemrev.8b00226.

[21] M.M. Bordbar, J. Tashkhourian, B. Hemmateenejad, Qualitative and quantitative analysis of toxic materials in adulterated fruit pickle samples by a colorimetric sensor array, Sens. Actuators B Chem. 257 (2018) 783–791, https://doi.org/10.1016/j.snb.2017.11.010.

[22] M.M. Bordbar, J. Tashkhourian, A. Tavassoli, E. Bahramali, B. Hemmateenejad, Ultrafast detection of infectious bacteria using optoelectronic nose based on metallic nanoparticles, Sens. Actuators B Chem. 319 (2020), https://doi.org/10.1016/j.snb.2020.128262.

[23] M.M. Bordbar, T.A. Nguyen, A.Q. Tran, H. Bagheri, Optoelectronic nose based on an origami paper sensor for selective detection of pesticide aerosols, Sci. Rep. 10 (2020), https://doi.org/10.1038/s41598-020-74509-8.

[24] M.M. Bordbar, H. Barzegar, J. Tashkhourian, M. Bordbar, B. Hemmateenejad, A non-invasive tool for early detection of acute leukemia in children using a paper-based optoelectronic nose based on an array of metallic nanoparticles, Anal. Chim. Acta 1141 (2021) 28–35, https://doi.org/10.1016/j.aca.2020.10.029.

[25] M. Chaharlangi, J. Tashkhourian, M.M. Bordbar, R. Brendel, P. Weller, B. Hemmateenejad, A paper-based colorimetric sensor array for discrimination of monofloral European honeys based on gold nanoparticles and chemometrics data analysis, Spectrochim. Acta Part A Mol. Biomol. Spectrosc. 247 (2021), https://doi.org/10.1016/j.saa.2020.119076.

[26] H. Sharifi, J. Tashkhourian, B. Hemmateenejad, A 3D origami paper-based analytical device combined with PVC membrane for colorimetric assay of heavy metal ions: application to determination of Cu(II) in water samples, Anal. Chim. Acta 1126 (2020) 114–123, https://doi.org/10.1016/j.aca.2020.06.006.

[27] H. Sharifi, J. Tashkhourian, B. Hemmateenejad, An array of metallic nanozymes can discriminate and detect a large number of anions, Sens. Actuators B Chem. 339 (2021), https://doi.org/10.1016/j.snb.2021.129911.

[28] P.J. Mazzone, J. Hammel, R. Dweik, J. Na, C. Czich, D. Laskowski, T. Mekhail, Diagnosis of lung cancer by the analysis of exhaled breath with a colorimetric sensor array, Thorax 62 (2007) 565–568, https://doi.org/10.1136/thx.2006.072892.

[29] E.R. Thaler, D.D. Lee, C.W. Hanson, Diagnosis of rhinosinusitis with a colorimetric sensor array, J. Breath Res. 2 (2008), https://doi.org/10.1088/1752-7155/2/3/037016.

[30] M.M. Bordbar, H. Samadinia, A. Sheini, J. Aboonajmi, H. Sharghi, P. Hashemi, H. Khoshsafar, M. Ghanei, H. Bagheri, A colorimetric electronic tongue for point-of-care detection of COVID-19 using salivary metabolites, Talanta 246 (2022), 123537.

[31] M. Asadi, E. Safaei, B. Ranjbar, L. Hasani, Thermodynamic and spectroscopic study on the binding of cationic ZD(II) and Co(II) tetrapyridinoporphyrazines to calf thymus DNA: the role of the central metal in binding parameters, New J. Chem. 28 (2004) 1227–1234, https://doi.org/10.1039/b404068f.

[32] E. Safaei, B. Ranjbar, L. Hasani, A study on the self assembly of Fe(II) and dual binding of Ni(II) porphyrazines on CT-DNA, J. Porphyr. Phthalocyanines 11 (2007) 805–814, https://doi.org/10.1142/S1088424607000928.

[33] B. Akhlaghinia, S. Tavakoli, M. Asadi, E. Safaei, N,N′,N″,N‴-tetramethyltetra-2,3-pyridinoporphyrazinato copper(II) methyl sulfate as a new and efficient catalyst for the dithioacetalization and the oxathioacetalization of carbonyl compounds, J. Porphyr. Phthalocyanines 10 (2006) 167–175, https://doi.org/10.1142/S108842460600020X.

[34] H. Sharghi, A.H. Nejad, Novel synthesis of meso-tetraarylporphyrins using CF3SO2Cl under aerobic oxidation, ChemInform 35 (2004), https://doi.org/10.1002/chin.200424113.

[35] D. Mansuy, Activation of alkanes: the biomimetic approach, Coord. Chem. Rev. 125 (1993) 129–141, https://doi.org/10.1016/0010-8545(93)85013-T.

[36] J. Bernadou, B. Meunier, A.S. Fabiano, A. Robert, "Redox Tautomerism" in high-valent metal-oxo-aquo complexes. Origin of the oxygen atom in epoxidation reactions catalyzed by water-soluble metalloporphyrins, J. Am. Chem. Soc. 116 (1994) 9375–9376, https://doi.org/10.1021/ja00099a083.

[37] A. Sheini, M.D. Aseman, M.M. Bordbar, Origami paper analytical assay based on metal complex sensor for rapid determination of blood cyanide concentration in fire survivors, Sci. Rep. 11 (2021), https://doi.org/10.1038/s41598-021-83186-0.
[38] M.M. Bordbar, B. Hemmateenejad, J. Tashkhourian, S.F. Nami-Ana, An optoelectronic tongue based on an array of gold and silver nanoparticles for analysis of natural, synthetic and biological antioxidants, Microchim. Acta 185 (2018), https://doi.org/10.1007/s00604-018-3021-1.
[39] K. Suslick, K. Hulkower, A. Sen, M. Sroka, W. McNamara, Method and apparatus for detecting ammonia from exhaled breath, US20050171449A1, 2005.
[40] K.S. Suslick, N.A. Rakow, A. Sen, Colorimetric artificial nose having an array of dyes and method for artificial olfaction, WO2001071318A1, 2001.
[41] V.N. Kopranenkov, E.A. Luk'yanets, Porphyrazines: synthesis, properties, application, Russ. Chem. Bull. 44 (1995) 2216–2232, https://doi.org/10.1007/BF00713584.
[42] B. Hemmateenejad, J. Tashkhourian, M.M. Bordbar, N. Mobaraki, Development of colorimetric sensor array for discrimination of herbal medicine, J. Iran. Chem. Soc. 14 (2017) 595–604, https://doi.org/10.1007/s13738-016-1008-6.
[43] J. Li, C. Hou, D. Huo, M. Yang, H.B. Fa, P. Yang, Development of a colorimetric sensor array for the discrimination of aldehydes, Sens. Actuators B Chem. 196 (2014) 10–17, https://doi.org/10.1016/j.snb.2014.01.054.
[44] S.H. Lim, C.J. Musto, E. Park, W. Zhong, K.S. Suslick, A colorimetric sensor array for detection and identification of sugars, Org. Lett. 10 (2008) 4405–4408, https://doi.org/10.1021/ol801459k.
[45] Z. Li, M. Fang, M.K. LaGasse, J.R. Askim, K.S. Suslick, Colorimetric recognition of aldehydes and ketones, Angew. Chem. 129 (2017) 9992–9995, https://doi.org/10.1002/ange.201705264.
[46] Y. Zhang, L.T. Lim, Colorimetric array indicator for NH3 and CO_2 detection, Sens. Actuators B Chem. 255 (2018) 3216–3226, https://doi.org/10.1016/j.snb.2017.09.148.
[47] A.C. Sedgwick, J.T. Brewster, T. Wu, X. Feng, S.D. Bull, X. Qian, J.L. Sessler, T. D. James, E.V. Anslyn, X. Sun, Indicator displacement assays (IDAs): the past, present and future, Chem. Soc. Rev. 50 (2021) 9–38, https://doi.org/10.1039/c9cs00538b.
[48] H. Khajehsharifi, M.M. Bordbar, A highly selective chemosensor for detection and determination of cyanide by using an indicator displacement assay and PC-ANN and its logic gate behavior, Sens. Actuators B Chem. 209 (2015) 1015–1022, https://doi.org/10.1016/j.snb.2014.10.053.
[49] M.M. Bordbar, J. Tashkhourian, B. Hemmateenejad, Structural elucidation and ultrasensitive analyses of volatile organic compounds by paper-based nano-optoelectronic noses, ACS Sens. 4 (2019) 1442–1451, https://doi.org/10.1021/acssensors.9b00680.
[50] B. Buszewski, A. Ulanowska, T. Ligor, N. Denderz, A. Amann, Analysis of exhaled breath from smokers, passive smokers and non-smokers by solidphase microextraction gas chromatography/mass spectrometry, Biomed. Chromatogr. 23 (2009) 551–556, https://doi.org/10.1002/bmc.1141.
[51] S.J. Davies, P. Španěl, D. Smith, Breath analysis of ammonia, volatile organic compounds and deuterated water vapor in chronic kidney disease and during dialysis, Bioanalysis 6 (2014) 843–857, https://doi.org/10.4155/bio.14.26.
[52] T. Saidi, O. Zaim, M. Moufid, N. El Bari, R. Ionescu, B. Bouchikhi, Exhaled breath analysis using electronic nose and gas chromatography–mass spectrometry for non-invasive diagnosis of chronic kidney disease, diabetes mellitus and healthy subjects, Sens. Actuators B Chem. 257 (2018) 178–188, https://doi.org/10.1016/j.snb.2017.10.178.
[53] J.J.B.N. Van Berkel, J.W. Dallinga, G.M. Möller, R.W.L. Godschalk, E.J. Moonen, E. F.M. Wouters, F.J.Van Schooten, A profile of volatile organic compounds in breath discriminates COPD patients from controls, Respir. Med. 104 (2010) 557–563, https://doi.org/10.1016/j.rmed.2009.10.018.

Mohammad Mahdi Bordbar received the Ph.D. degrees in analytical chemistry from Shiraz University (2018). He has appointed as a postdoctoral researcher at chemical injuries research center, Baqiyatallah University of Medical Sciences. His research is focused on fabrication of optical electronic nose and optical electronic tongue for food, environmental and biological applications.

Hossein Samadinia is currently MD/Ph.D. of Medical Nanotechnology at the Chemical Injuries Research Center, Baqiyatallah University of Medical Sciences.

Ali Hajian is a researcher with background in chemistry and microsystems engineering and many years of experience in research both at universities and in industry in Germany and Austria. His main research interests are electrochemical sensors and supercapacitors, glass ceramics and surface technologies. .

Azarmidokht Sheini is currently Assistant Professor of Analytical Chemistry. Her activities concern the construction of different optical sensors/biosensors and their application in analytical matrices. Her current research interests are in the field of fabrication of paper based sensors based on nanoparticles and nanoclusters for diagnosis of chronic diseases.

Elham Safaei is Associate Professor of Inorganic Chemistry at Department of Chemistry, Shiraz University, Shiraz, Iran. Her activities concern on bioinorganic chemistry, catalyst synthesis and performance evaluation.

Jasem Aboonajmi received the BSC degree in applied chemistry from Firoozabad Islamic Azad University in 2009, M. Sc. and Ph.D. degrees in organic chemistry from Sistan and Baluchestan University (2013) and Shiraz University (2019), respectively. His research interests include synthesis of *N*-heterocyclic compounds, synthesis and reactions of allenes and amino acids, asymmetric multi-component reactions, green chemistry, synthesis and characterization of bioactive ligands and nano catalysts. At the moment, his current research involves the synthesis and reaction of catechols.

Fabiana Arduini is Associated Professor at Department of Chemical Science and Technologies, University of Rome "Tor Vergata", CEO of start-up SENSE4MED, DG at ISO9001 Certified Laboratory LabCap, University of Rome "Tor Vergata", Associated Editor of Microchemical Journal, Elsevier, Specialty Chief Editor in Micro- and Nano Sensors, Frontiers in Sensors and Coordinator of Italian Sensor Group, Italian Chemical Society 2019 – 2021. Her research activity deals with the development of miniaturized electrochemical devices mainly using screen-printed electrodes modified with nanomaterials and paper-based analytical tools applied in environmental, biomedical, and defense sectors, with over 167 articles published in peer-review journals, H index 47, Scopus source, > 5 patents, coordinators of several national/international projects. Her name is present in PLoS Biology 2019 https://doi.org/10.1371/journal.pbio.3000384 which listed the top 2% most cited researchers in the world.

Hashem Sharghi is Professor of Organic Chemistry at Chemistry Department of Shiraz University. He received the BSC degree in chemistry from Tabriaz University, Iran (1973), M. Sc. degrees in chemistry and polymer from University of Aston in Birmingham, England (1977) and Ph. D. degrees in organic chemistry from University of Manchester in Manchester, England (1988), respectively. His research interests cover the synthesis of heterocyclic compounds, bioactive ligands and complexes such as (Porphyrins, Salens, Crown ethers), nano catalysts, coupling reactions, multi-component reactions. In 2011, he received the Organic Chemistry Award of the Iranian Chemical Society. Also, he won the Allameh Tabatabai Award from the National Elite Foundation of Iran in 2015.

Pegah Hashemi received her Ph.D. in Analytical Chemistry in 2018 at Bu-Ali Sina University, Hamedan, Iran. She is currently a Post-doctoral researcher in the field of fabrication of electrochemical biosensors and latheral-flow kit at Research and Development Department, Farin Behbood Tashkhis LTD, Tehran, Iran.

Hosein Khoshsafar received a Ph.D. in Analytical Chemistry from the Bu-Ali Sina University, Hamedan, Iran. His current research is focused on sensors, biosensors and development and fabrication of lateral flow tests for Healthcare, Food safety and Environmental monitoring.

Mostafa Ghanei obtained his M.D. in medicine in 1988, and obtained his specialty certification in internal medicine in 1993 from Esfahan University of Medical Sciences, Esfahan, Iran. He has been practicing as a pulmonologist since 1997. He has many articles in the field of basic and clinical aspects of respiratory diseases and is one of the most distinguished researchers in the field of chemical inhalation toxicology.

Hasan Bagheri is currently a Professor of Analytical Chemistry. His activities concern the construction of different optical and electrochemical sensors/biosensors and their application in analytical matrices. His current research interests are in the field of fabrication of electrochemical sensors/biosensors and lateral flow kits based on new nanomaterials.